



HAL
open science

MULTISCALE FOURTH-ORDER MODELS FOR IMAGE INPAINTING AND LOW-DIMENSIONAL SETS RECOVERY

Zakaria Belhachmi, Moez Kallel, Maher Moakher, Anis Theljani

► **To cite this version:**

Zakaria Belhachmi, Moez Kallel, Maher Moakher, Anis Theljani. MULTISCALE FOURTH-ORDER MODELS FOR IMAGE INPAINTING AND LOW-DIMENSIONAL SETS RECOVERY. 2016. hal-01114292v2

HAL Id: hal-01114292

<https://hal.science/hal-01114292v2>

Preprint submitted on 3 Feb 2016 (v2), last revised 9 Feb 2016 (v3)

HAL is a multi-disciplinary open access archive for the deposit and dissemination of scientific research documents, whether they are published or not. The documents may come from teaching and research institutions in France or abroad, or from public or private research centers.

L'archive ouverte pluridisciplinaire **HAL**, est destinée au dépôt et à la diffusion de documents scientifiques de niveau recherche, publiés ou non, émanant des établissements d'enseignement et de recherche français ou étrangers, des laboratoires publics ou privés.

MULTISCALE FOURTH-ORDER MODEL FOR IMAGE INPAINTING AND LOW-DIMENSIONAL SETS RECOVERY

ZAKARIA BELHACHMI

*Mathematics, Information Technology and Applications Laboratory,
University of Haute Alsace, France.
zakaria.belhachmi@uha.fr*

MOEZ KALLEL

*IPEIT, University of Tunis,
2, Rue Jawaher Lel Nehru, 1089 Montfleury, Tunisia.
moez.kallel@ipeit.rnu.tn*

MAHER MOAKHER

*National Engineering School at Tunis, University of Tunis El-Manar,
B.P. 37, 1002 Tunis-Belvédère, Tunisia.
maher.moakher@gmail.com*

ANIS THELJANI

*National Engineering School at Tunis, University of Tunis El-Manar,
B.P. 37, 1002 Tunis-Belvédère, Tunisia.
thalianianis@gmail.com*

Received (Day Month Year)
Revised (Day Month Year)
Communicated by (xxxxxxxxxx)

We consider fourth-order variational models for image inpainting problems, with emphasis on the recovery of low-order sets (edges, corners) and the curvature. The approach consists of constructing a family of regularized functionals and to select, locally and in an adaptive way, the regularization parameters which control the diffusion of the reconstruction operator. Unlike the usual methods which optimize the parameters a priori and lead, in general, to complex systems of PDEs, our approach is based on a continuous, linear, high-order diffusion model that is dynamically adjusted at the discrete level. We analyze the method in the framework of the calculus of variations and the Γ -convergence tools and we show that it yields results that might be expected from more complex systems of PDEs. We obtain simple discrete algorithms based on mixed-finite elements. We present several numerical examples to test our approach and to make some comparisons with existing methods.

Keywords: Image inpainting; Inverse problems; Regularization procedures; Mixed finite elements.

AMS Subject Classification: 65M32, 65M50, 65M22, 94A08, 65N22, 35G15, 35Q68

1. Introduction

Digital image inpainting started with the works of engineers and computer scientists in the mid-nineties of last century. It refers to restoring a scratched or damaged image with missing information. This type of image processing task is very important and has many applications in various fields (painted canvas and movies restoration, augmented reality, etc). Let $\Omega \subset \mathbb{R}^2$ denotes the entire image domain, the basic idea in image inpainting is to fill-in an incomplete/damaged region $D \subset \Omega$ based upon the image information available outside D (i.e., in $\Omega \setminus D$) in such a manner, that a viewer can not detect the restored parts. Different techniques have been applied to solve this problem. Among them, Partial Differential Equations (PDEs) are widely used and are proven to be efficient for solving several image processing problems ^{11,12,15,24,25,27,31,33,34}. The underlying idea of PDE-based methods is to interpolate image data across the boundaries of the missing region D using a great variety of partial differential diffusion equations. Various second-order diffusion equations have been proposed in the literature ^{15,25,27}. They have the advantage of being well-established theoretically and easy to solve numerically. However, their major drawbacks are the disconnection of level lines over large distances (Connectivity Principle), the smooth propagation of edges into the damaged domain or the inability of reproducing features of higher order (curvature, corners,...) of the initial image due to the lack of information (second-order). Besides, these classical methods do not work when the damaged region D touches the boundary of Ω . In such a situation, the authors in ³¹ proposed a relevant and specialized inpainting method. Unusual boundary conditions were considered and inpainting was then achieved by an extrapolation process from one side of D by means of a nonlinear Cauchy problem in view of the space variable.

The shortcomings of second-order methods gave rise to a new class of higher-order diffusion models which in general perform better. In fact, whenever the image is contaminated by noise, higher-order PDEs, specially linear ones, damp the noise faster than second-order based diffusion models. In addition, they give the possibility of including information about the curvature (which is of third-order) of edges in the equation. Moreover, they allow matching edges across large distances because the supplementary information about edge directions which can be provided by the use of boundary conditions for both the solution and its derivatives.

Overview on higher-order PDE models

Bertalmio *et al.* ¹² pioneered a two dimensional fourth-order PDE which consists in propagating both the gradient direction (geometry) and the gray-scale values of the image inside the region to be filled by solving the following equation:

$$\partial_t u - \nabla^\perp \cdot \nabla \Delta u = 0, \text{ in } D, \quad u = f, \text{ on } \partial D, \quad (1.1)$$

where ∇^\perp denotes the perpendicular gradient $(-\partial_y, \partial_x)$ and f is the initial damaged image. This model was the subject of other improvements in ¹¹ based on the Navier-

Stokes equations for fluid dynamics.

Inspired by the elastica model ^{34,36}, T. Chan *et al.* proposed in ³⁷ to approach the Euler-elastica functional by considering the following functional:

$$\|u - f\|_{L^2(\Omega)} + \int_K (a + b\kappa^2) d\mathcal{H}^1(x), \quad (1.2)$$

where \mathcal{H}^1 is the Hausdorff measure, K is a closed regular subset of Ω and $\kappa = \nabla \cdot (\nabla u / |\nabla u|)$ is the curvature of level sets $\gamma_r := \{x \in K \mid u(x) = r\}$ and a , b are two positive constant weights. It is a higher-order variational model where the regularization term combines the total variation, sensitive to the length of the isolines, and the square of the curvature, which favors curved lines than straight ones. Minimizing (1.2) leads to a highly nonlinear PDE and therefore its numerical solution is a non trivial task. It was the subject of many numerical investigations ^{2,26,27,32}. In the same spirit, Esedoglu and Shen proposed in ²⁷ the Mumford-Shah-Euler image inpainting model which is a high-order correction of the Mumford-Shah model by incorporating the Willmore energy. They gave an efficient numerical realization based on the Γ -convergence approximations of Ambrosio and Tortorelli ^{3,4}, and De Giorgi ²⁹.

Bertozzi *et al.* exploited in ¹⁴ the Cahn-Hilliard equation for binary image inpainting. It is a semilinear fourth-order PDE originally introduced in material sciences by John W. Cahn and John E. Hilliard in ²⁰ and it describes the evolution of an interface separating two stable states. The $TV - H^{-1}$ model was proposed in ¹⁹ as a generalization of Cahn-Hilliard equation to gray-scale images.

The multiscale approach

Most high-order approaches to the inpainting problem make use of the minimization of an energy of Willmore type, i.e., (1.2). However, the models obtained this way are generally highly nonlinear and difficult to solve numerically. In another hand, the easiest way to obtain a fourth-order PDE is to minimize $\int_D |\Delta u|^2 dx$ which has several interests in image processing and various works are focusing on minimizing this energy. It was considered by Blake and Zisserman in ¹⁶ and afterwards in ^{21,38} to overcome the limitations of the Mumford-Shah functional (which is of second-order). Its major benefit is that it leads to the fourth-order PDE:

$$\Delta^2 u = 0, \text{ in } D, \quad u = f \quad + \text{ another boundary condition on } \partial D. \quad (1.3)$$

This isotropic fourth-order (stationary) diffusion equation is richer than second order ones and has the benefits of connecting edges across (large) missing parts while preserving the curvature. However, because of its strong smoothing effect, it cannot capture important features of the image like corners, edges, etc.

In this paper, we consider a multiscale approach to construct functionals based

on fourth-order PDEs (1.3). More precisely, we consider the following equation:

$$\begin{cases} \partial_t u + \Delta(\Delta_\alpha u) + \lambda_D(u - f) = 0, & \text{in } \mathbb{R}_+ \times \Omega, \\ u = \Delta_\alpha u = 0, & \text{on } \mathbb{R}_+ \times \partial\Omega, \\ u(0, x) = f, & \text{in } \Omega, \end{cases} \quad (1.4)$$

where $\Delta_\alpha u = \operatorname{div}(\alpha(x)\nabla u)$ and $\lambda_D = \lambda_0 \chi_{\Omega \setminus D}$ for $\lambda_0 \gg 0$ and $\chi_{\Omega \setminus D}$ is the indicator function of the sub-domain $\Omega \setminus D$. The values of the diffusion function α , which encodes different scales in the image, are dynamically and locally chosen in order to control the amount of smoothing of the operator. Note that the homogeneous boundary condition for u is not a restrictive condition and general boundary data can be handled by a lifting operator.

It is known that linear diffusion models are not well-suited for capturing fine geometric structures of an image (edges, corners). However, we prove in this paper that our approach allows to restore such fine features. The reason of this ‘‘apparent paradox’’ is that the adaptive process which is the key of the method, is in fact nonlinear. We construct a nonlinear discrete approximation to a continuous linear model, this allows for a dynamical ‘‘adaptation of the model’’ during the processes to make it sensitive to low-order sets and fine features. In addition, the process turns out to be convergent, in the Γ -convergence sense, to a Willmore-like functional. Thus, with this approach, we combine, at the same framework, the simplicity of the linear diffusion model for the image inpainting and, the necessary, nonlinear process for the selection of the diffusion coefficient to capture the singularities.

Organization of the paper

The remainder of this paper is organized as follows: In Section 2, we prove by standard variational techniques and a fixed point approach the existence of H^1 -solution for the image inpainting problem. We obtain our equation from a minimization problem –of the regularized functional– based on an H^{-1} -fidelity term. In Section 3, we describe in details the adaptive strategy. In particular, we show that it is a two-step approach where, first a mesh-adaptation based on metric error indicator is used to fit the geometry of the computed solution, and second a residual type error indicator is used to locally select the value of α . We perform a Γ -convergence analysis of this process and we show that the solution u generated by the adaptive strategy approximates a solution of a new model which combines the Mumford-Shah functional and the H^{-1} -fidelity term. In Section 4, we recall the Cahn-Hilliard equation for image inpainting in order to make a comparison with our model. Finally, in Section 5 we implement our approach and treat several numerical examples to test its efficiency and robustness.

2. Image inpainting problem

We study in this section the image inpainting problem by considering the system (1.4). For the sake of clarity, in the rest of the paper we omit the time dependence

of functions and we use the notation u instead of $u(t)$.

2.1. H^1 -weak solution of the stationary equation

Assume that Ω is a bounded open set of \mathbb{R}^2 with piecewise smooth boundary $\partial\Omega$. We recall that the operator Δ^{-1} is the inverse of the negative Laplacian with homogeneous Dirichlet boundary conditions, i.e., $u = \Delta^{-1}g$ is the unique solution of:

$$\begin{cases} -\Delta u = g, & \text{in } \Omega, \\ u = 0, & \text{on } \partial\Omega. \end{cases} \quad (2.1)$$

Let $H^{-1}(\Omega)$ be the dual space of $H_0^1(\Omega)$ with corresponding norm $\|u\|_{-1} = \|\nabla\Delta^{-1}u\|_2$ and inner product $\langle u, v \rangle_{-1} = \langle \nabla\Delta^{-1}u, \nabla\Delta^{-1}v \rangle_2$, where $\langle \cdot, \cdot \rangle_2$ and $\|\cdot\|_2$ are the classical inner product and its corresponding norm in the space $L^2(\Omega)$.

We consider the solution of the following stationary problem:

$$\begin{cases} \Delta(\Delta_\alpha u) + \lambda_D(u - f) = 0, & \text{in } \Omega, \\ u = \Delta_\alpha u = 0, & \text{on } \partial\Omega, \end{cases} \quad (2.2)$$

which can be seen as stationary solution of (1.4). Problem (2.2) can be rewritten as follows:

$$\begin{cases} \Delta_\alpha u + \Delta^{-1}(\lambda_D(f - u)) = 0, & \text{in } \Omega, \\ u = \Delta_\alpha u = 0, & \text{on } \partial\Omega, \end{cases} \quad (2.3)$$

or equivalently as a coupled elliptic system:

$$\begin{cases} -\Delta_\alpha u = w, & \text{in } \Omega, \\ -\Delta w = \lambda_D(f - u), & \text{in } \Omega, \\ u = w = 0, & \text{on } \partial\Omega. \end{cases} \quad (2.4)$$

The weak formulation of problem (2.3) is: Find $u \in H_0^1(\Omega)$ such that:

$$\langle \alpha \nabla u, \nabla \phi \rangle_2 - \langle (\lambda_D(f - u)), \phi \rangle_{-1} = 0, \quad \forall \phi \in H_0^1(\Omega). \quad (2.5)$$

Throughout the paper, we suppose that the domain Ω is partitioned into I disjoint sub-domains $(\Omega_\ell)_\ell$ such that α is given by the piecewise constant scalar function:

$$\alpha = \alpha_\ell, \quad \text{in } \Omega_\ell, \quad \ell = 1, \dots, I.$$

We denote $\alpha_m = \min_{1 \leq \ell \leq I} \alpha_\ell > 0$ and $\alpha_M = \max_{1 \leq \ell \leq I} \alpha_\ell$.

Note that even if $f \in L^2(\Omega)$, from the elliptic regularity results, one has $w \in H^2 \cap H_0^1(\Omega)$ however, the solution u might be only $H_0^1(\Omega)$ since α is only bounded and measurable. In fact, we recall the following regularity result for the operator $-\text{div}(\alpha \nabla(\cdot))$:⁸

Proposition 2.1. *There exists a constant c depending only on the geometry of Ω , such that a weak solution u of the associated Dirichlet problem belongs to $H^{s+1}(\Omega)$, for all real numbers $s < s_0$, where s_0 is given by:*

$$s_0 = \min \left\{ \frac{1}{2}, c \left| \log \left(1 - \frac{\alpha_m}{\alpha_M} \right) \right| \right\}.$$

Following the methodology used in ¹⁹, we now prove the existence of the H^1 -weak solution of the stationary problem by means of Schauder's fixed-point theorem.

Proposition 2.2 (Schauder's fixed-point theorem ²⁸). *Let X be a Banach space and $K \subset X$ be a compact and convex set of X . Assume that the operator $T : K \rightarrow K$ is continuous. Then T admits a fixed point.*

For $R > 0$, to be chosen later, we define the convex set:

$$V = \{u \in H_0^1(\Omega); \|u\|_2 \leq R\},$$

and we consider the following minimization problem:

$$\min_{u \in H_0^1(\Omega)} \mathcal{J}(u, v), \quad (2.6)$$

where

$$\mathcal{J}(u, v) = \begin{cases} \int_{\Omega} \frac{\alpha(x)}{2} |\nabla u|^2 dx + \frac{1}{2\lambda_0} \|\lambda_0 u - \lambda_D f - \Lambda_D v\|_{-1}^2, & \text{if } u \in V, \\ +\infty, & \text{otherwise,} \end{cases} \quad (2.7)$$

with f and $v \in L^2(\Omega)$ and where $\Lambda_D = \lambda_0 - \lambda_D$.

Proposition 2.3. *Let $v \in L^2(\Omega)$, the functional $\mathcal{J}(\cdot, v)$ admits a unique minimizer $u \in V$.*

Proof. The functional $\mathcal{J}(\cdot, v)$ is strictly convex. In fact, let u_1 and u_2 be two functions in $H_0^1(\Omega)$ such that $u_1 \neq u_2$ and $t \in]0, 1[$, we have:

$$\begin{aligned} & t\mathcal{J}(u_1, v) + (1-t)\mathcal{J}(u_2, v) - \mathcal{J}(tu_1 + (1-t)u_2, v) \\ &= \frac{t(1-t)}{2} \left[\int_{\Omega} \alpha(x) |\nabla u_1|^2 dx + \int_{\Omega} \alpha(x) |\nabla u_2|^2 dx - 2 \int_{\Omega} \alpha(x) \nabla u_1 \cdot \nabla u_2 dx \right] \\ &+ \frac{t(1-t)}{2\lambda_0} \left[\|\lambda_0 u_1 - \lambda_D f - \Lambda_D v\|_{-1}^2 + \|\lambda_0 u_2 - \lambda_D f - \Lambda_D v\|_{-1}^2 \right] \\ &- \frac{t(1-t)}{\lambda_0} \left[\int_{\Omega} \nabla \Delta^{-1}(\lambda_0 u_1 - \lambda_D f - \Lambda_D v) \cdot \nabla \Delta^{-1}(\lambda_0 u_2 - \lambda_D f - \Lambda_D v) dx \right] \\ &= \frac{t(1-t)}{2} \int_{\Omega} \alpha(x) |\nabla(u_1 - u_2)|^2 dx + \frac{t(1-t)}{2\lambda_0} \|\lambda_0(u_1 - u_2)\|_{-1}^2 > 0. \end{aligned}$$

Furthermore, $\mathcal{J}(\cdot, v)$ is weakly lower semi-continuous in $H^1(\Omega)$. We consider a minimizing sequence $(u_n)_{n \in \mathbb{N}}$ of $\mathcal{J}(\cdot, v)$, i.e.,

$$\mathcal{J}(u_n, v) \xrightarrow{n \rightarrow \infty} \inf_{u \in V} \mathcal{J}(u, v) = L.$$

Then, there is a constant $M > 0$ such that $\int_{\Omega} \alpha(x) |\nabla u_n|^2 dx \leq M$ for all $n \geq 0$, and also we have $\|u_n\|_2 \leq R$ (otherwise $\mathcal{J}(u_n, v)$ would not be finite). Then, using the boundedness of $\alpha(x)$, we get that the sequence $(u_n)_{n \in \mathbb{N}}$ is uniformly bounded in $H^1(\Omega)$. Therefore, there exists a subsequence, still denoted $(u_n)_{n \in \mathbb{N}}$, such that $u_n \rightharpoonup u$ weakly in $H^1(\Omega)$ and $u_n \xrightarrow[n \rightarrow \infty]{} u$ in $L^2(\Omega)$, with $\|u\|_2 \leq R$. Thanks to the continuity of the operator $\Delta^{-1} : H^{-1}(\Omega) \rightarrow L^2(\Omega)$, we get:

$$\mathcal{J}(u, v) \leq \liminf_{n \rightarrow \infty} \mathcal{J}(u_n, v).$$

The limit u is then a minimizer for $\mathcal{J}(\cdot, v)$. Uniqueness is guaranteed by the strict convexity of $\mathcal{J}(\cdot, v)$. \square

The Euler-Lagrange equation corresponding to (2.6) reads:

$$\begin{cases} -\Delta_{\alpha} u - \Delta^{-1}(\lambda_D(f - u) + \Lambda_D(v - u)) = 0, & \text{in } \Omega, \\ u = \Delta^{-1}(\lambda_D(f - u) + \Lambda_D(v - u)) = 0, & \text{on } \partial\Omega. \end{cases} \quad (2.8)$$

Its weak formulation is: Find $u \in H_0^1(\Omega)$ such that:

$$\langle \alpha \nabla u, \nabla \phi \rangle_2 - \langle (\lambda_D(f - u) + \Lambda_D(v - u)), \phi \rangle_{-1} = 0, \quad \forall \phi \in H_0^1(\Omega). \quad (2.9)$$

Let $T : L^2(\Omega) \rightarrow L^2(\Omega)$ be the operator such that $T(v) = u$ where u is the unique solution of (2.9). Therefore, if there exists a fixed point $u = v$ of the operator, it will be a solution of problem (2.5).

Proposition 2.4. *The operator T admits a fixed point $u \in V$. Moreover, u is H^1 -weak solution of the equation (2.2).*

Proof. Let $v \in B(0, R)$ (where $B(0, R)$ denotes the ball in $L^2(\Omega)$ with center 0 and radius R). From Proposition 2.3, the minimization problem (2.7) admits a unique minimizer $u = T(v)$ in the space $H^1(\Omega)$ such that $u \in B(0, R)$. Since the embedding $H^1(\Omega) \hookrightarrow L^2(\Omega)$ is compact, the operator T then maps $L^2(\Omega) \rightarrow K$, where K is a compact subset of $L^2(\Omega)$. Thus we have:

$$T : B(0, R) \rightarrow B(0, R) \cap K = \tilde{K},$$

where \tilde{K} is a compact and convex subset of $L^2(\Omega)$. To apply Schauder's fixed-point theorem, it remains to prove that T is continuous in $B(0, R)$. Let $(v_k)_{k \geq 0}$ be a sequence which converges to $v \in L^2(\Omega)$ and $T(v_k) = u_k$. The function u_k is then the unique minimizer of (2.7) associated with v_k , and we have: $\mathcal{J}(u_k, v_k) \leq \mathcal{J}(0, v_k)$, i.e.,

$$\mathcal{J}(u_k, v_k) \leq \frac{1}{2\lambda_0} \|\lambda_D f + \Lambda_D v_k\|_{-1}^2.$$

Since $L^2(\Omega) \hookrightarrow H^{-1}(\Omega)$, we get $\|v_k\|_{-1} \leq C \|v_k\|_{L^2(\Omega)} \leq CR$ and also $\|\lambda_D f\|_{-1} \leq C'$ for some given constants $C, C' > 0$. Accordingly, we obtain the following estimate:

$$\mathcal{J}(u_k, v_k) \leq C' + CR^2,$$

and then $(u_k)_{k \geq 0}$ is uniformly bounded in $H^1(\Omega)$. Thus, we can consider a convergent subsequence $u_{k_j} \xrightarrow{j \rightarrow \infty} u \in H^1(\Omega)$ and $u_{k_j} \xrightarrow{j \rightarrow \infty} u$ in $L^2(\Omega)$. Hence, the unique (weak) solution $T(v_k) = u_k$ of:

$$\begin{cases} -\Delta_\alpha u_k - \Delta^{-1}(\lambda_D(f - u_k) + \Lambda_D(v_k - u_k)) = 0, & \text{in } \Omega, \\ u_k = \Delta^{-1}(\lambda_D(f - u_k) + \Lambda_D(v_k - u_k)) = 0, & \text{on } \partial\Omega, \end{cases}$$

weakly converges to the unique weak solution u of (2.8). From the uniqueness of the solution in V , we obtain $u = T(v)$. We then deduce that T is continuous in $L^2(\Omega)$ and the existence of a stationary solution u follows from Schauder's fixed-point theorem. In addition, this solution satisfies (2.3), or equivalently, is a stationary solution of the problem (1.4). \square

Remark 2.1. The solution u of equation (2.2) verifies the estimate:

$$\alpha_m \|\Delta u\|_2 + \frac{\lambda_0}{2} \|u\|_2 \leq \frac{\lambda_0}{2} \|f\|_2.$$

Therefore, we may choose $R = \|f\|_2$.

2.2. The evolution equation

Now, observe that the previous existence proof of a stationary solution applies to show that the following unbounded operator (in L^2):

$$A(u) = \Delta(\Delta_\alpha u) + \lambda_D u,$$

is maximal. Moreover, we have:

$$\langle A(u), u \rangle_2 \geq \sum_{\ell=1}^I \alpha_m \langle \Delta u, \Delta u \rangle_{L^2(\Omega_\ell)} + \langle \lambda_D u, u \rangle_2 \geq 0,$$

which means that it is monotone. Thus it follows from the theory of maximal monotone operators¹⁸, that the evolution problem (1.4) admits a unique solution $u \in L^2(0, T; H_0^1(\Omega) \cap H^1(0, T; H^{-1}(\Omega))) \cap C([0, T]; L^2(\Omega))$.

As in the stationary case, problem (1.4) can be splitted into two second-order equations by introducing an auxiliary function w such that:

$$\begin{cases} \partial_t u - \Delta w + \lambda_D(u - f) = 0, & \text{in } \mathbb{R}_+ \times \Omega, \\ -\Delta_\alpha u = w, & \text{in } \mathbb{R}_+ \times \Omega, \\ u = w = 0, & \text{on } \mathbb{R}_+ \times \partial\Omega, \\ u(0, x) = f(x), & \text{in } \Omega. \end{cases} \quad (2.10)$$

The weak formulation reads then:

Find a pair $(u, w) \in L^2(0, T; H_0^1(\Omega) \cap H^1(0, T; H^{-1}(\Omega))) \times L^2(0, T; H_0^1(\Omega))$, $u(0, x) = f(x)$, such that:

$$\begin{cases} \langle \partial_t u, \phi \rangle_2 + \langle \nabla w, \nabla \phi \rangle_2 + \langle \lambda_D u, \phi \rangle_2 = \langle \lambda_D f, \phi \rangle_2, & \forall \phi \in H_0^1(\Omega), \\ \langle \alpha \nabla u, \nabla \psi \rangle_2 - \langle w, \psi \rangle_2 = 0, & \forall \psi \in H_0^1(\Omega). \end{cases} \quad (2.11)$$

Let u the solution of problem (1.4). Then, it is easy to verify that the pair $(u, -\Delta_\alpha u)$, is a weak solution of (2.11). We consider another solution $(u_1, w_1) \in H_0^1(\Omega) \times H_0^1(\Omega)$ of the system (2.11), we then have:

$$\begin{cases} \langle \partial_t(u - u_1), \phi \rangle_2 + \langle \nabla(w - w_1), \nabla \phi \rangle_2 + \langle \lambda_D(u - u_1), \phi \rangle_2 = 0, & \forall \phi \in H_0^1(\Omega), \\ \langle \alpha \nabla(u - u_1), \nabla \psi \rangle_2 - \langle (w - w_1), \psi \rangle_2 = 0, & \forall \psi \in H_0^1(\Omega). \end{cases}$$

Let $(\zeta_\ell)_{\ell=1}^I$ be a partition of unity associated to the decomposition $(\Omega_\ell)_1^I$, and picking $\psi = \alpha_\ell^{-1} \zeta_\ell(w - w_1)$, in the second equation, we have the identity:

$$\int_{\Omega_\ell} \alpha_\ell^{-1} \zeta_\ell (w - w_1)^2 dx = \int_{\Omega_\ell} \alpha_\ell \nabla(u - u_1) \alpha_\ell^{-1} \nabla \zeta_\ell (w - w_1) dx, \quad \forall \ell = 1, \dots, I. \quad (2.12)$$

Summing up, we get:

$$\sum_{\ell=1}^I \alpha_\ell^{-1} \int_{\Omega_\ell} \zeta_\ell (w - w_1)^2 dx = \int_{\Omega} \nabla(u - u_1) \nabla(w - w_1) dx \geq 0. \quad (2.13)$$

By choosing the test function $\phi = u - u_1$ in the first equation and using (2.13) and the positivity of λ_D , we obtain:

$$\langle \partial_t(u - u_1), u - u_1 \rangle_2 = -\langle \nabla(u - u_1), \nabla(w - w_1) \rangle_2 - \langle \lambda_D(u - u_1), (u - u_1) \rangle_2 \leq 0.$$

So that

$$\partial_t(\|u(t) - u_1(t)\|_2^2) = 2\langle \partial_t(u - u_1), u - u_1 \rangle_2 \leq 0.$$

It follows that the function $t \mapsto \|u(t) - u_1(t)\|_2^2$ is decreasing on \mathbb{R}_+ . Since $u(0) = u_1(0)$, we get $u = u_1$ which implies that $w = w_1$. Thus, problems (1.4) and (2.11) are equivalent.

2.3. Discretization

For the discretization of the time derivative $\partial_t u$, we use the forward Euler scheme.

Let $\frac{u - u^{old}}{\Delta t}$ be an approximation of $\partial_t u$, where Δt is a time step, u^{old} and u are the solutions at time t_{old} and $t = t_{old} + \Delta t$, respectively. Therefore, time discretization together with splitting scheme (2.10) leads to the following time-stepping problem:

$$\begin{cases} \langle \frac{u - u^{old}}{\Delta t}, \phi \rangle_2 + \langle \nabla w, \nabla \phi \rangle_2 + \langle \lambda_D u, \phi \rangle_2 = \langle \lambda_D f, \phi \rangle_2, & \forall \phi \in H_0^1(\Omega), \\ \langle \alpha \nabla u, \nabla \psi \rangle_2 - \langle w, \psi \rangle_2 = 0, & \forall \psi \in H_0^1(\Omega). \end{cases} \quad (2.14)$$

Proposition 2.5. *For a fixed $u^{old} \in H_0^1(\Omega)$, the problem (2.14) admits a solution $(u, w) \in H_0^1(\Omega) \times H_0^1(\Omega)$.*

Proof. For a given $v \in L^2(\Omega)$, $u^{old} \in H_0^1(\Omega)$ and $\Delta t > 0$, we define:

$$\lambda'_D = \lambda_D + \frac{1}{\Delta t} \quad \text{and} \quad f' = \frac{1}{\lambda'_D} \left(\lambda_D f + \frac{u^{old}}{\Delta t} \right).$$

We then consider the following problem:

$$\begin{cases} -\Delta_\alpha u - \Delta^{-1}(\lambda'_D(f' - u)) = 0, & \text{in } \Omega, \\ u = \Delta_\alpha u = 0, & \text{on } \partial\Omega. \end{cases} \quad (2.15)$$

Using the same reasoning as in Proposition 2.3, we can prove the existence of H^1 -solution of (2.15) such that the pair $(u, -\Delta_\alpha u)$ satisfies the system (2.14). To prove uniqueness, let $(u_1, w_1) \in H_0^1(\Omega) \times H_0^1(\Omega)$ be another solution of the system (2.14), we then have:

$$\begin{cases} \langle \nabla(w - w_1), \nabla\phi \rangle_2 + \langle \lambda'_D(u - u_1), \phi \rangle_2 = 0, & \forall \phi \in H_0^1(\Omega), \\ \langle \alpha \nabla(u - u_1), \nabla\psi \rangle_2 - \langle (w - w_1), \psi \rangle_2 = 0, & \forall \psi \in H_0^1(\Omega). \end{cases}$$

Reasoning like for the system (2.11) and using the inequality (2.13), we obtain:

$$\langle \lambda'_D(u - u_1), (u - u_1) \rangle_2 = -\langle \nabla(u - u_1), \nabla(w - w_1) \rangle_2 \leq 0.$$

From the positivity of λ'_D , we get:

$$\langle \lambda'_D(u - u_1), (u - u_1) \rangle_2 = 0.$$

From the positivity of λ'_D , it follows that $u = u_1$. Therefore, w and w_1 solve following problem:

$$\begin{cases} -\Delta w + \lambda'_D(u - f') = 0, & \text{in } \Omega, \\ w = 0, & \text{on } \partial\Omega, \end{cases} \quad (2.16)$$

which clearly admits a unique solution and consequently $w = w_1$. \square

3. Discrete problem and adaptive strategy

We assume that the domain Ω is polygonal and we consider a regular family of triangulations \mathbb{T}_h made of element which are triangles (or quadrilaterals) with a maximum size h , satisfying the usual admissibility assumptions, i.e., the intersection of two different elements is either empty, a vertex, or a whole edge. For $h > 0$, we introduce the following discrete space:

$$X_h = \{v_h \in C(\bar{\Omega}) | \forall K \in \mathbb{T}_h, v_h|_K \in P_1(K)\} \cap H_0^1(\Omega).$$

The discretized version of the splitted problem (2.11) leads to finding a pair $(u_h, w_h) \in X_h \times X_h$ solution of:

$$\begin{cases} \langle \frac{u_h - u_h^{old}}{\Delta t}, \phi_h \rangle_2 + \langle \nabla w_h, \nabla\phi_h \rangle_2 + \langle \lambda_D u_h, \phi_h \rangle_2 = \langle \lambda_D f_h, \phi_h \rangle_2, & \forall \phi_h \in X_h, \\ \langle \alpha \nabla u_h, \nabla\psi_h \rangle_2 - \langle w_h, \psi_h \rangle_2 = 0, & \forall \psi_h \in X_h, \end{cases} \quad (3.1)$$

where f_h is a finite element approximation of f associated with \mathbb{T}_h . Since $X_h \subset H_0^1(\Omega)$, the well-posedness of the problem (3.1) follows from (2.14).

3.1. Adaptive procedure

For each element $K \in \mathbb{T}_h$, the following local discrete energy:

$$\eta_K = \alpha_K^{\frac{1}{2}} \|\nabla u_h\|_{L^2(K)}, \quad (3.2)$$

contains some information on the error distribution of the computed solution u_h . In fact, the discontinuities (edges) are contained in regions where the brightness changes sharply and consequently where this error indicator is large. Moreover, it may be proven that the gradient of u_h captures this change in brightness and its magnitude provides an information about the “strength” of the edges (see ⁹). Thus, the quantity (3.2) acts as an edge detector and locates such regions. Furthermore, this local error indicator is in some sense equivalent to the energy norm mostly used as an edge detection in the topological gradient based-methods ^{5,6,7}. This particularity makes it well suited to control and locally select the diffusion coefficient α using the following algorithm:

Algorithm 1

- (1) Start with the initial grid \mathbb{T}_h^0 corresponding to the image.
- (2) **Adaptive steps:**
 - Compute u_h^0 on \mathbb{T}_h^0 with a large constant $\alpha = \alpha^0$.
 - Build an adapted mesh \mathbb{T}_h^1 (in the sense of the finite element method, i.e., with respect to the parameter h) with a metric error indicator.
 - In triangles where η_K is large (with respect to its mean value), we perform a local choice of $\alpha(x)$ on \mathbb{T}_h^1 to obtain a new function $\alpha^1(x)$.
- (3) Go to steps 1. and 2. and compute u_h^1 on \mathbb{T}_h^1 .

During the adaptation, we use the following formula for each triangle K :

$$\alpha_K^{k+1} = \max \left(\frac{\alpha_K^k}{1 + \tau * \left(\left(\frac{\eta_K}{\|\eta\|_\infty} \right) - 0.1 \right)^+}, \alpha_{trh} \right), \quad (3.3)$$

where α_{trh} is a threshold parameter and τ is a coefficient which controls the rate of decrease in α , $u^+ = \max(u, 0)$. Here η is the piecewise-constant function such that $\eta|_K = \eta_k$, $\forall K \in \mathbb{T}_h^1$.

Remark 3.1. There are other possible choices for this formula as it will appear in the Γ -convergence analysis. The one given here is the one implemented for the numerical computations. Loosely speaking, it may be viewed as follows: in regions of high gradients, it decreases the values of α when the error indicator deviates more than 10% from its mean value. α decreases nearly as a geometric sequence with the iteration number, until a given threshold is attained.

Let us give more details on the implementation of this algorithm. First, we build an adapted mesh \mathbb{T}_h^1 as follows: close to the jump sets of u_h , the error is large, we then cut the element K into a finite number of smaller elements to decrease such an error and to fit the edges, while, far from these jump sets, there is no restriction on how to choose the triangles and the initial grid is coarsened. The adopted meshes have small number of degrees of freedom in the homogeneous regions which makes the method considerably fast. Second, we perform an “optimal” choice of the function α following the map furnished by the error indicator $(\eta_K)_{K \in \mathbb{T}_h}$, on each element K and in accordance with (3.3) in order to correctly approximate edges.

Remark 3.2. It is easily seen that if u wants to jump across a triangle K then η_K tends to $+\infty$ and thus α_K is chosen such that it tends to 0. If η_K tends to 0, then α_K remains constant, otherwise η_K tends to 0 and α_K remains constant. The overall decrease of the global error is guaranteed by a balance between the energy in these two parts of the domain. Chosen this way, the function α plays in the present context a role similar to that of the z -field in the Ambrosio-Tortorelli approximation³ for the Mumford-Shah energy³⁵.

3.2. Γ -convergence analysis for the adaptive algorithm

In this section, we motivate our approach by analyzing the limit behavior of the solution generated by the adaptive algorithm. More precisely, we want to prove that this approach allows to approximate, in the Γ -convergence sense, a new model that couples a Mumford-Shah function with an H^{-1} -term, which we will call MS- H^{-1} .

Γ -convergence analysis A Γ -convergence study of this adaptive strategy was presented in¹⁰ for optic flow estimation. The authors proved that this algorithm is equivalent to the adaptive one introduced by Chambolle-Dal Maso²³ and Chambolle-Bourdin²² where a numerical discrete approximation of the Mumford-Shah energy was proposed. This approach, based on finite-element discretization and adaptive mesh strategy, is a good approximation, in the Γ -convergence sense¹⁷ of the Mumford-Shah energy³⁵ (see²³ for more details). We briefly recall the results and the numerical approximation of this method. For a fixed angle $0 < \theta_0 \leq 2\pi/3$, a constant $c \geq 6$, and for $\epsilon > 0$, let $\mathcal{T}_\epsilon(\Omega) = \mathcal{T}_\epsilon(\Omega; \theta_0; c)$ be the set of all triangulations of Ω whose triangles K have the following characteristics:

- (i) The length of each of the three edges of K is between ϵ and ϵc .
- (ii) The three angles of K are greater than or equal to θ_0 .

Let $V_\epsilon(\Omega)$ be the set of all continuous functions $u : \Omega \rightarrow \mathbb{R}$ such that u is affine on each triangle K of a triangulation $\mathbb{T} \in \mathcal{T}_\epsilon(\Omega)$. For a given u , we define $\mathcal{T}_\epsilon(u) \subset \mathcal{T}_\epsilon(\Omega)$ as the set of all triangulations adapted to the function u , i.e., such that u is piecewise affine on \mathbb{T} . We consider a non-decreasing continuous function $g : [0, +\infty) \rightarrow$

$[0, +\infty)$ such that:

$$\lim_{t \rightarrow 0} \frac{g(t)}{t} = 1, \quad \lim_{t \rightarrow +\infty} g(t) = g_\infty < +\infty.$$

For any $u \in L^p(\Omega)$, ($p \geq 1$) and $\mathbb{T} \in \mathcal{T}_\epsilon(\Omega)$, the authors in ²³ introduced the following minimization problem:

$$G_\epsilon(u) = \min_{\mathbb{T} \in \mathcal{T}_\epsilon(\Omega)} \tilde{G}_\epsilon(u, \mathbb{T}), \quad (3.4)$$

where

$$\tilde{G}_\epsilon(u, \mathbb{T}) = \begin{cases} \sum_{K \in \mathbb{T}} |K \cap \Omega| \frac{1}{h_K} g(h_K |\nabla u|^2), & u \in V_\epsilon(\Omega), \mathbb{T} \in \mathcal{T}_\epsilon(\Omega), \\ +\infty, & \text{otherwise.} \end{cases}$$

When ϵ goes to zero and provided θ_0 is less than some $\Theta > 0$, it was proven that the energy G_ϵ Γ -converges to the Mumford-Shah functional:

$$G(u) = \begin{cases} \int_{\Omega} |\nabla u(x)|^2 dx + g_\infty \mathcal{H}^1(S_u), & u \in L^2(\Omega) \cap GSBV(\Omega), \\ +\infty, & u \in L^2(\Omega) \setminus GSBV(\Omega), \end{cases}$$

where is $GSBV(\Omega)$ the generalized special function of bounded variation (see ¹).

Remark 3.3. If $F : X \rightarrow [-\infty, +\infty]$ is continuous and $(G_\epsilon)_\epsilon$ Γ -converges to G then $(F + G_\epsilon)_\epsilon$ Γ -converges to $F + G$.

From the result of the Γ -convergence of G_ϵ to G , see ²³, the continuity of the second term of the functional in $L^2(\Omega)$ (which follows from the continuity of Δ^{-1} , i.e., the stability in the elliptic problems) and Remark 3.3, we have:

Proposition 3.1. *Let f and v in $L^2(\Omega)$ be two given functions and $\epsilon > 0$ be a positive parameter. Therefore, the sequence of functionals*

$$G_\epsilon(u_\epsilon) + \frac{1}{2\lambda_0} \|\lambda_0 u_\epsilon - \lambda_D f - (\lambda_0 - \lambda_D)v\|_{-1}^2,$$

Γ -converges for $\epsilon \rightarrow 0$ in the topology of $L^2(\Omega)$ to

$$G(u) + \frac{1}{2\lambda_0} \|\lambda_0 u - \lambda_D f - (\lambda_0 - \lambda_D)v\|_{-1}^2.$$

Let ψ be the Legendre-Fenchel transform of g . For a given triangulation \mathbb{T}_ϵ , it was proven in ²³ that the minimization of G_ϵ is equivalent to the minimization of the following functional:

$$G'_\epsilon(u, v, \mathbb{T}_\epsilon) = \sum_{K \in \mathbb{T}_\epsilon} |K \cap \Omega| \frac{1}{h_K} \left(v_K |\nabla u|^2 + \frac{\psi(v_K)}{h_K} \right),$$

over all $u \in V_\epsilon(\Omega)$ and $v = (v_K)_{K \in \mathbb{T}_\epsilon}(\Omega)$, piecewise constant on each $K \in \mathbb{T}_\epsilon$. For a fixed u , the minimizer over each v is explicitly given by:

$$v_K = g'(h_K |\nabla u|^2). \quad (3.5)$$

The adaptive strategy presented in this paper is then similar to the iterative method used in ²³ and the local choice of α using the error indicator η_K is similar of the choice of v_K in (3.5) with $v = \alpha$.

Remark 3.4.

- The analysis presented here is carried out with the Neumann boundary conditions on u , which is the framework used in ^{10,22,23} for a denoising problem or optic flow estimation. The application to the Dirichlet case requires some (tedious but non-essential) modifications and the result still holds.
- Note that, like for second-order models, different PDE-based approaches might yield a Γ -limit approximation of the Mumford-Shah model. Given a function α , the computation of the solution u is simple and fast. In fact, after each adaptation step the number of nodes of the adapted mesh can be reduced.

4. Cahn-Hilliard equation

For the sake of completeness, we will make a comparison with the Cahn-Hilliard model ^{13,14,15} that we now recall. The Cahn-Hilliard equation ²⁰ originally refers to John W. Cahn and John E. Hilliard ²⁰ and was introduced to phenomenologically describe phase separation, i.e., the change from one state to another. It is a fourth-order semi-linear PDE and is obtained as the H^{-1} -gradient flow of the following Ginzburg-Landau energy:

$$\frac{1}{2} \int_{\Omega} |\nabla u|^2 dx + \frac{1}{\epsilon^2} W(u), \quad (4.1)$$

where phase separation is modeled by the smooth free energy, e.g., double-well potentials W such that:

$$W(u) = (1 - u^2)u^2, \quad (4.2)$$

or a non-smooth free energy as follows:

$$W(u) = \psi(u) + I_{[0,1]}(u), \quad (4.3)$$

where $\psi(u) = \frac{1}{2}u(1-u)$, and $I_{[0,1]}(u) := \begin{cases} \frac{1}{2}u(1-u), & 0 \leq u \leq 1, \\ +\infty, & \text{otherwise.} \end{cases}$

The analogy between the Cahn-Hilliard model in material sciences and Cahn-Hilliard model in image inpainting is that the two state phases are considered as two homogeneous regions and the interface is considered as an edge. In image inpainting, it was exploited by Bertozzi *et al.* in ¹⁴ and afterwards in ^{13,15,19} by considering the following equation:

$$\begin{cases} \partial_t u + \Delta(\epsilon \Delta u - \frac{1}{\epsilon} W'(u)) + \lambda_D(u - f) = 0, & \text{in } \mathbb{R}^+ \times \Omega, \\ u = f \text{ and } \epsilon \Delta u - \frac{1}{\epsilon} W'(u) = 0, & \text{on } \mathbb{R}^+ \times \partial\Omega, \\ u(0, x) = f, & \text{in } \Omega, \end{cases} \quad (4.4)$$

which was obtained by incorporating the data fidelity term $\lambda_D(f - u)$. Note that the classical Chan Hilliard equation (4.4) is only appropriate for two-scale (binary) images inpainting due to the double well potential W which vanishes on only the values 0 and 1.

Remark 4.1. For the time discretization of Cahn-Hilliard equation, we use a convexity splitting scheme (see ^{15,19}). The idea is to divide the energy functional into two parts; a convex part plus a concave one. The convex part is then treated implicitly while the concave part is treated explicitly.

5. Numerical experiments

In this work, all the PDEs are solved with the open source software FreeFem++³⁰. In all examples, the damaged/missed regions are delimited by the red contour. We give some examples for the application of our proposed approach to image inpainting. The goal is to reconstruct the missing information in the red parts, i.e., D , by the diffusion of the information from the intact part, i.e., $\Omega \setminus D$. In all examples, we set $\lambda_0 = 10^7$, and $\Delta t = 0.1$ and an initial guess $u(0, x) = 0.5, \forall x \in D$.

Curvature inpainting. We present the numerical results for the adaptive inpainting approach in order to illustrate the effectiveness of the proposed algorithm for the inpainting of curvature. In Fig. 1, we present the reconstruction of quarter of a circle. We display the evolution of the restored image for iterations 1, 5 and 20. In the first iteration (α is constant), we solved a biharmonic equation which gives a curved, but a very smooth (blurred), edge in D . By iterations, we can see the efficiency of the adaptation process in the damaged region where the edge was inpainted sharply by simultaneously keeping its curvature.

Other examples are presented in Fig. 2 and Fig. 4. The curvature in Fig. 2 is well inpainted which proves that our approach, based on fourth-order linear diffusion model, allows us to obtain a very interesting result that one might expect by solving complex PDEs like the Euler's elastica³⁷, which is highly nonlinear and numerically difficult to solve. We give in Fig. 5 a zoom caption in the damaged region 2 which proves that the missing part is well restored and is very close to the original one.

"Real world"-image inpainting. The experiments in Fig. 6 show the efficiency of the proposed method in a real image inpainting. The portions of unknown pixels are 45%, 55% and 75%, respectively. From these experiments, we can see that the proposed model can successfully recover the inpainting domain even when up to 75% of pixels are unknown.

Comparison with the Cahn-Hilliard model. In Fig. 7, we have chosen the same image presented by Bertozzi, Esedoglu and Gillette (see ¹⁴). We give the result obtained by solving the Cahn-Hilliard equation and the one obtained using our approach. We display the evolution of the restored image at iteration 1, 5 and 10 which show that the edges are progressively and sharply approximated and the four corners are very accurately matched. Notice that the image for Cahn-Hilliard equation is computed in a two-steps process. In the first step, the authors solved

their equation with a large value of ϵ , e.g., $\epsilon = 0.1$, until the numerical scheme is close to a steady state. In this step, the level lines are continued into the missing domain. In a second step, they used the previous result as an initial time condition u_0 for a smaller ϵ (e.g., $\epsilon = 0.01$) in order to sharpen the contours. This is an adaptive choice for ϵ , however, subjected to a hand tuning and being uniform in the entire domain.

Broken three bars. In Fig. 8, we show the inpainting result for a synthetic image which represents three broken bars forming a T -junction. We give the restored images using total variation, harmonic and biharmonic models, respectively. As expected, total variation inpainting model is unable to connect the edges between the three bars because it does not fulfill the connectivity principle. Harmonic and biharmonic inpainting models produce a smooth solution u in D , blurring the edges. However, the proposed approach is able to sharply connect the edges between three bars while enforcing the curvature.

6. Conclusion

In this paper, we have investigated a multiscale fourth-order diffusion PDE for image inpainting. The continuous model is linear and variational. We introduced an adaptive approximation procedure which is nonlinear, but completely a posteriori strategy, e.g. the selection of the diffusion coefficient is based upon information on the computed solutions during the solution steps. We analyzed our approach from the variational point of view and we established its connections with a Mumford-Shah-like energy, in the sense of the Γ -convergence. We have implemented the considered model to test the method, we have also made some comparisons with existing approaches to demonstrate its capabilities. We have underlined, in the presented tests, the good quality in the recovery of low dimensional sets (edges, corners) and curvature in the inpainted zone. We emphasize that in our approach the adaptive selection of the diffusion coefficients is:

- (i) Automatic, i.e., no external intervention on the algorithm.
- (ii) Objective and a posteriori, i.e., the scale of α (the way to decrease its values) is explicitly obtained from computable quantities (error indicators) which are very sensitive to the singularities of the solution.
- (iii) Local, i.e., at each location in the computation domain (finite-element cell, thus the pixel scale).
- (iv) Low cost, thanks to the coarsening of the mesh in the homogeneous parts of the domain.

In addition, the method may be improved straightforwardly by considering α the diffusion function as a matrix which introduces some anisotropy in the models and the overall approach is easy to implement in the framework of variational methods of approximation and remains compatible with most existing variational models.

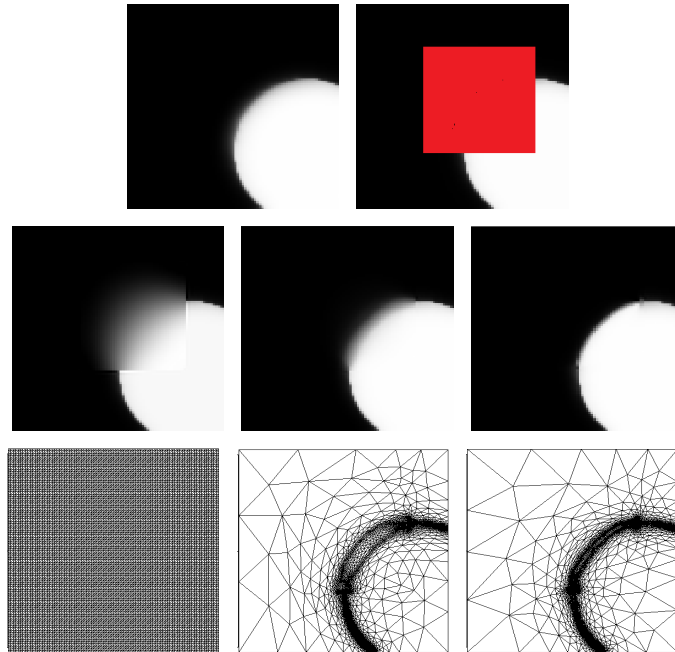


Fig. 1. Top row: Original and damaged images. Middle row: Restored image using the model (1.4) and adaptation at iterations 1, 5 and 20, respectively. Bottom row: Mesh evolution at iterations 1, 5 and 20, respectively.



Fig. 2. From left to right: Original, damaged and restored images using model (1.4) and adaptation.

References

1. L. AMBROSIO, N. FUSCO, AND D. PALLARA, *Functions of Bounded Variation and Free Discontinuity Problems*, Oxford Mathematical Monographs, 2000.
2. L. AMBROSIO AND S. MASNOU, *A direct variational approach to a problem arising in image reconstruction*, Interfaces and Free Boundaries, 5 (2003), pp. 63–81.
3. L. AMBROSIO AND M. TORTORELLI, *Approximation of functional depending on jumps by elliptic functional via γ -convergence*, Comm. Pure Appl. Math., 43 (1990), pp. 999–1036.
4. ———, *On the approximation of free discontinuity problems*, Boll. Un. Mat. Ital., 6 (1992), pp. 105–123.

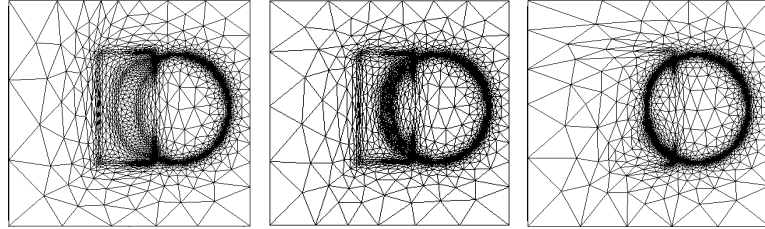


Fig. 3. Mesh evolution at iterations 2, 5 and 10, respectively.

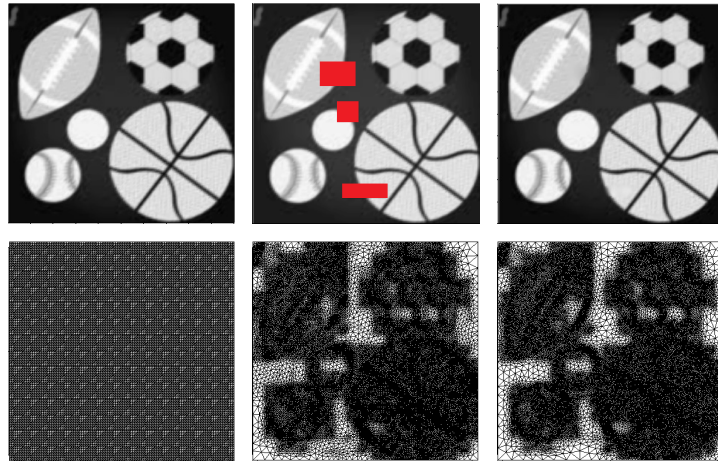


Fig. 4. Top row: Original, damaged and restored images using model (1.4) and adaptation., respectively. Bottom row: The evolution of the mesh at iterations 1, 5 and 20, respectively.

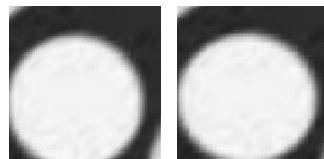


Fig. 5. Zoom on the damaged region 2: Original and restored.

5. D. AUROUX, L. JAAFAR BELAID, AND B. RJAIBI, *Application of the topological gradient method to color image restoration*, SIAM Journal on Imaging Sciences, 3 (2010), pp. 153–175.
6. D. AUROUX, L-D. COHEN, AND M. MASMOUDI, *Contour detection and completion for inpainting and segmentation based on topological gradient and fast marching algorithms*, Journal of Biomedical Imaging, vol. 2011 (2011).
7. D. AUROUX AND M. MASMOUDI, *Image processing by topological asymptotic expansion*, Journal of Mathematical Imaging and Vision, 33 (2009), pp. 122–134.
8. Z. BELHACHMI, C. BERNARDI, AND A. KARAGEORGHIS, *Mortar spectral element dis-*

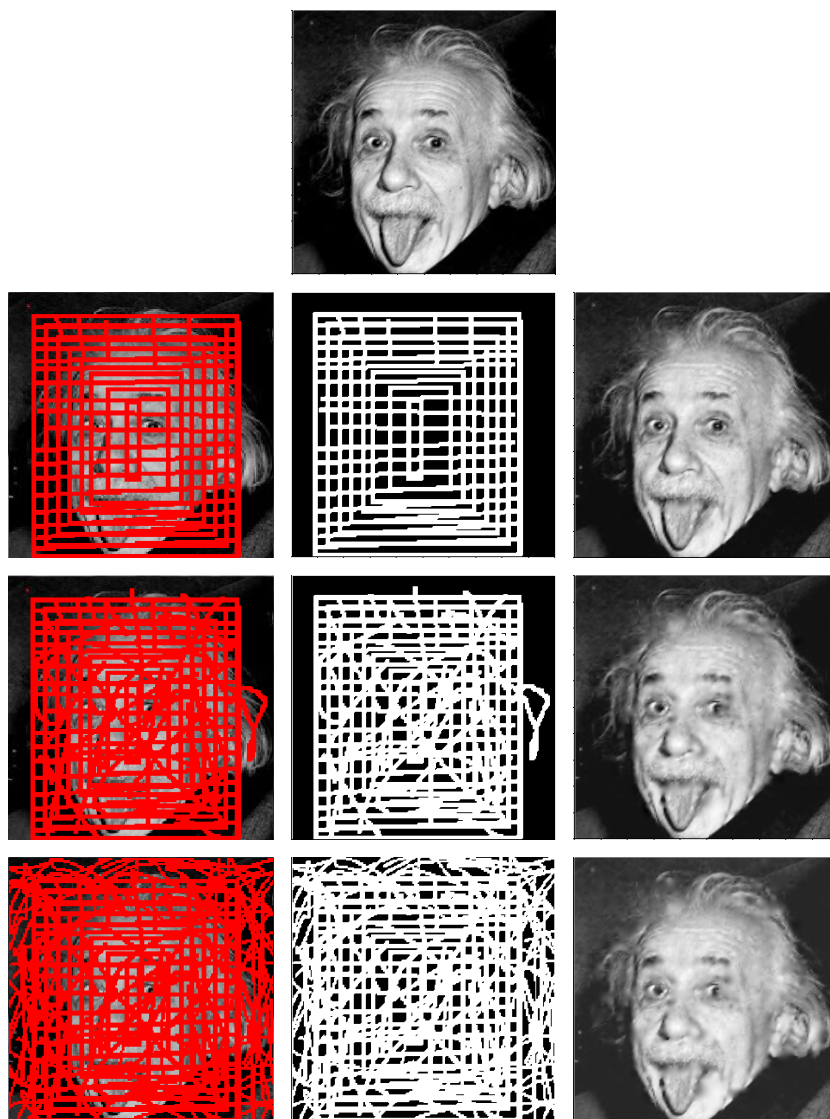


Fig. 6. The damaged, mask and restored images, respectively. Over: 45% of pixels are damaged- Middle: 55% of pixels are damaged. Below: 75% of pixels are damaged.

cretization of nonhomogeneous and anisotropic Laplace and Darcy equations, M2AN, 41 (2007), pp. 801–824.

9. Z. BELHACHMI AND F. HECHT, *Control of the effects of regularization on variational optic flow computations*, Journal of Mathematical Imaging and Vision, 40 (2011), pp. 1–19.
10. ———, *An adaptive approach for segmentation and TV edge-enhancement in the optic flow estimation*, Submitted, (2015).

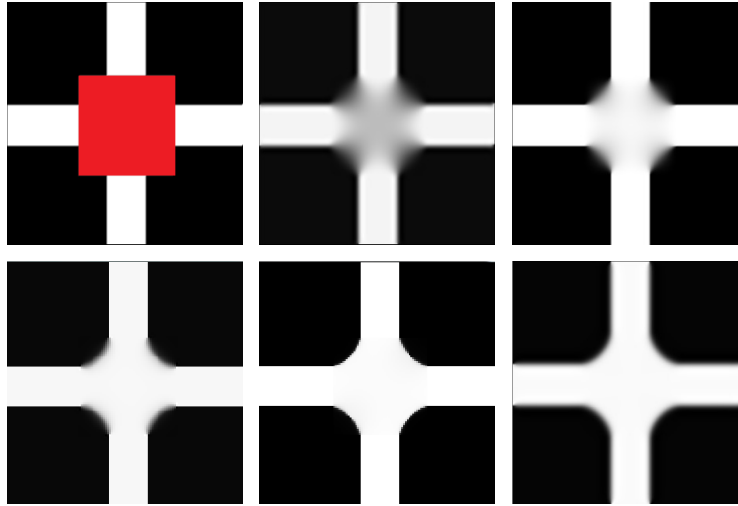


Fig. 7. Top row: Damaged and restored images using model (1.4) and adaption (iterations 1 and 5). Bottom row: Restored images using model (1.4) and adaption (iterations 10 and 20) and Cahn-Hilliard model.



Fig. 8. Top row: Damaged image and restored ones using total variation and harmonic models, respectively. Bottom row: Restored images using biharmonic model and our approach at iterations 5 and 20, respectively.

11. M. BERTALMIO, A. L. BERTOZZI, AND G. SAPIRO, *Navier-Stokes, fluid dynamics, and image and video inpainting*, in Proc. IEEE Computer Vision and Pattern Recognition (CVPR), 2001, pp. 355–362.
12. M. BERTALMIO, G. SAPIRO, V. CASELLES, AND C. BALLESTERI, *Image inpainting*, in Proceedings of the 27th Annual Conference on Computer Graphics and Interactive Techniques, New York, 2000, ACM, pp. 417–427.

13. A. BERTOZZI, S. ESEDOGLU, AND A. GILLETTE, *Analysis of a two-scale Cahn-Hilliard model for image inpainting*, Multiscale Modeling and Simulation, 6 (2007), pp. 913–936.
14. ———, *Inpainting of binary images using the Cahn-Hilliard equation*, IEEE Trans. Image Proc., 16 (2007), pp. 285–291.
15. A. BERTOZZI AND C.-B. SCHONLIEB, *Unconditionally stable schemes for higher order inpainting*, Communications in Mathematical Sciences, 9 (2011), pp. 413–457.
16. A. BLAKE AND A. ZISSERMAN, *Visual Reconstruction*, MIT Press, Cambridge, MA, USA, 1987.
17. A. BRAIDES, *Gamma-Convergence for Beginners*, vol. 22 of Oxford Lecture Series in Mathematics and its Applications, Oxford University Press, 2002.
18. H. BRÉZIS, *Opérateurs Maximaux Monotones et Semi-Groupes de Contractions dans les Espaces de Hilbert*, North-Holland Mathematics Studies, North Holland New-York, Amsterdam, London, 1973.
19. M. BURGER, L. HE, AND C.-B. SCHNLIEB, *Cahn-Hilliard inpainting and a generalization for grayvalue images*, SIAM J. Imaging Sci., 2 (2009), pp. 1129–1167.
20. J. CAHN AND E. HILLIARD, *Free energy of a nonuniform system. I. Interfacial free energy*, Journal of Chemical Physics, 28 (1958).
21. M. CARRIERO, A. LEACI, AND F. TOMARELLI, *Free gradient discontinuity and image inpainting*, Journal of Mathematical Sciences, 161 (2012), pp. 805–819.
22. A. CHAMBOLLE AND B. BOURDIN, *Implementation of an adaptive finite-element approximation of the Mumford-Shah functional*, Numer. Math., 85 (2000), pp. 609–646.
23. A. CHAMBOLLE AND G. DAL MASO, *Discrete approximation of the Mumford-Shah functional in dimension two*, M2AN Math. Model. Numer. Anal., 33 (1999), pp. 651–672.
24. T. CHAN AND J. SHEN, *Non-texture inpainting by curvature-driven diffusion (CDD)*, J. Visual Comm. Image Rep., 12 (2001), pp. 436–449.
25. ———, *Mathematical models for local non-texture inpainting*, SIAM Journal on Applied Mathematics, 62 (2002), pp. 1019–1043.
26. G. CHUNG, J. HAHN, AND X. TAI, *A fast algorithm for Euler’s elastica model using augmented Lagrangian method*, SIAM Journal on Imaging Sciences, 4 (2011), pp. 313–344.
27. S. ESEDOGLU AND J. SHEN, *Digital image inpainting by Mumford-Shah-Euler model*, European Journal of Applied Mathematics, 13 (2002), pp. 353–370.
28. L. C. EVANS, *Partial Differential Equations*, vol. 19 of Graduate Studies in Mathematics, American Mathematical Society, Providence, Rhode Island, 1998.
29. E. DE GIORGI, *Some remarks on γ -convergence and least squares methods*, in Composite Media and Homogenization Theory, G. Dal Maso and G. F. Dell’Antonio, eds., Birkhauser Boston, Cambridge, MA, (1991), pp. 135–142.
30. F. HECHT, *New development in freefem++*, Journal of Numerical Mathematics, 20 (2002), pp. 251–265.
31. M. KALLEL, M. MOAKHER, AND A. THELJANI, *The Cauchy problem for a nonlinear elliptic equation: Nash-game approach and application to image inpainting*, Inverse Problems and Imaging, 9 (2015), pp. 853–874.
32. S. MASNOU, *Filtrage et désocclusion d’images par méthodes d’ensembles de niveau*, PhD thesis, Université Paris-Dauphine, 1998.
33. S. MASNOU, *Disocclusion a variational approach using level lines*, IEEE Transactions on Image Processing, 11 (2002), pp. 68–67.
34. S. MASNOU AND J. M. MOREL, *Level-lines based disocclusion*, Proceedings of 5th IEEE International Conference on Image Processing, (1998), pp. 259–264.

35. D. MUMFORD AND J. SHAH, *Optimal approximations by piecewise smooth functions and associated variational problems*, Communications on Pure and Applied Mathematics, 42 (1989), pp. 577–685.
36. M. NITZBERG, D. MUMFORD, AND T. SHIOTA, *Filtering, segmentation and depth*, vol. 662 of Lecture Notes in Computer Science. Springer, (1993).
37. J. SHEN, S. H. KANG, AND T. CHAN, *Euler's elastica and curvature-based inpainting*, SIAM J. Imaging Sci., 63 (2002), pp. 564–592.
38. M. ZANETTI AND A. VITTI, *The Blake-Zisserman model for digital surface models segmentation*, ISPRS Annals of Photogrammetry, Remote Sensing and Spatial Information Sciences, vol. II-5/W2, (2013), pp. 355–360.